Pattern formation on the edge of chaos: Experiments with CO oxidation on a Pt(110) surface under global delayed feedback

Matthias Bertram, Carsten Beta, Michael Pollmann, Alexander S. Mikhailov, Harm H. Rotermund, and Gerhard Ertl
Fritz-Haber-Institut der Max-Planck-Gesellschaft, Faradayweg 4-6, 14195 Berlin, Germany
(Received 2 December 2002; published 25 March 2003)

Experiments with catalytic oxidation of carbon monoxide on Pt(110) show that chemical turbulence in this system can be suppressed by application of appropriate global delayed feedback. Different spatiotemporal patterns, seen near the transition from turbulence to uniform oscillations, are investigated. Such patterns include intermittent turbulence, oscillatory standing waves, cellular structures, and phase clusters. Using a method based on the Hilbert transform, spatial distributions of local phase and amplitude in these patterns are reconstructed from the experimental data.

DOI: 10.1103/PhysRevE.67.036208 PACS number(s): 82.40.Bj, 82.40.Np, 05.45.Jn

I. INTRODUCTION

Control of chaos is one of the central problems in nonlinear dynamics. In contrast to existing exact methods [1], a heuristic approach based on the introduction of delayed feedbacks does not require extensive real-time computations [2]. For extended systems, where spatially resolved access is difficult, global delayed feedbacks can be employed. In such methods, information continuously gathered from all elements of the system is summed up and used to generate a signal which is applied back to control a common system parameter. Global feedbacks can be employed to stabilize otherwise unstable trajectories, but also as a tool to produce new spatiotemporal patterns. Action of global feedbacks on chaotic extended systems has been experimentally or theoretically investigated for lasers [3], gas discharge devices [4], semiconductors [5,6], populations of electrochemical oscillators [7], and surface chemical reactions [8]; it was also discussed in the more general context of the complex Ginzburg-Landau equation [9,10]. Furthermore, various forms of global feedback have been successfully applied to control pattern formation in nonchaotic excitable [11,12] and oscillatory [13–17] chemical systems.

Nonequilibrium systems on the edge of chaos are capable of generating a broad variety of complex patterns. To bring a system to a boundary between periodic and chaotic dynamics, its parameters may be appropriately chosen or external forcing may be introduced. However, a practical implementation of such predefined control meets serious difficulties because a system at the edge of chaos is sensitive even to small parameter variations. An alternative is provided by using global delayed feedback. The advantage of this method is that an acting force is generated by the system itself and therefore automatically adjusts to the variations of experimental conditions.

In this paper, we apply a global delayed feedback to investigate spatiotemporal pattern formation near the transition to chaos in an oscillatory surface chemical reaction. We demonstrate that chemical turbulence can be suppressed by means of such a feedback and that various types of chaotic and nonchaotic patterns can be induced. The system we consider is the catalytic oxidation of carbon monoxide on Pt(110), representing the best studied example among oscillatory surface reactions (see Ref. [18] for a review of such systems).

Under low-pressure conditions, the CO oxidation on platinum single-crystal surfaces proceeds via a Langmuir-Hinshelwood mechanism [19]. Due to a high energy barrier in the gas phase, molecules of CO and oxygen have to adsorb on the catalytic surface before the reaction can take place. The adsorption of oxygen is dissociative. Adsorbed CO molecules are bound to the surface considerably less strongly than oxygen atoms and hence may desorb as well as diffuse on the surface, while these processes are negligible for oxygen under typical reaction conditions. Produced carbon dioxide almost immediately desorbs into the gas phase, leaving again free space for adsorption. On Pt(110), temporal oscillations of the reaction rate are possible due to an adsorbate-driven phase transition in the top substrate layer [20]. Under such oscillatory conditions, the interplay between reaction and diffusion processes leads to the development of a rich variety of spatiotemporal patterns, including rotating spiral waves, target patterns, and chemical turbulence [21].

In a previous publication [8], initial experiments on suppression of turbulence by global delayed feedback in catalytic CO oxidation have been reported. In this paper, we present the results of more detailed investigations. Under systematic variation of both feedback parameters, the feedback intensity and the delay time, we find additional, previously undiscovered types of feedback-induced patterns. For cluster patterns, we also investigate effects of a variation of the feedback window. The various complex spatiotemporal structures observed are analyzed by making use of a technique based on the Hilbert transform.

The paper is organized as follows. The experimental setup and the feedback method are introduced in the following section. In Sec. III, the results of our experimental investigations are shown. The properties of each type of feedback-induced pattern are described in detail. Then, in Sec. IV, the observed patterns are further characterized by the time-dependent spatial distributions of their local oscillation phase and amplitude. The paper ends with a discussion of the obtained results in Sec. V.

II. EXPERIMENTAL SETUP

In our experiments, the Pt(110) single-crystal sample was kept in an ultrahigh-vacuum (UHV) apparatus. Controlled

supply of reactants into the UHV chamber was enabled by an automated dosing system that allowed to keep the partial pressures of gases constant within a maximal variation of 0.1%. Only purified gases (CO 4.7, O_2 5.6) have been used. The partial pressures under reaction conditions (up to 10^{-3} mbar) were measured by means of a differentially pumped quadrupole mass spectrometer. Preceding each series of experiments, the sample has been prepared by repeated cycles of Ar ion sputtering below 470 K and subsequent annealing to 750 K.

As a consequence of mass balance, global gas phase coupling is generally present in surface chemical reactions [18]. Its effects in CO oxidation on Pt(110) have been studied both theoretically [22–24] and experimentally [25]. To minimize the effects of such internal coupling, specially prefabricated single crystals have been used. About 80% of the Pt(110) single-crystal surface (10 mm in diameter) has been covered by microlithographic deposition with Ti. The Ti layer was then oxidized in the reaction chamber, thereby producing a TiO_2 layer which is catalytically inactive for the considered reaction. Only the free Pt areas remained active. In this way, isolated surface reactors of various sizes could be created. For the experiments, reactive areas of about 1 mm^2 have been chosen.

For the visualization of spatiotemporal adsorbate patterns on the catalytic surface, photoemission electron microscopy (PEEM) [26] was used. This method produces real-time images of the lateral distribution of adsorbed species on the surface. More precisely, the distribution of photoelectron emission from the surface under ultraviolet light irradiation is displayed. The yield of photoelectrons depends sensitively on the local work function φ of the substrate, which is changed due to the presence of adsorbates. Compared to the free Pt(110) surface, a monolayer of oxygen coverage increases the work function by $\Delta\varphi \approx 0.8$ eV, thereby strongly decreasing the brightness of PEEM images. Full CO coverage also increases the work function but produces a smaller effect ($\Delta\varphi \approx 0.3$ eV). In our experiments, the PEEM instrument has been used to monitor a surface area of ≈ 500 μm in diameter. The spatial resolution of the images was about 1 μm. A frame rate of 25 camera images per second guaranteed a sufficiently good temporal resolution of the PEEM recordings. Standard image processing including background subtraction, contrast-brightness adjustments, and image averaging has been performed to improve the signal-to-noise ratio of the images.

Global delayed feedback was introduced into the system via the gas phase by making the instantaneous dosing rate of CO gas dependent on real-time properties of the developing patterns. While monitoring the patterns on the surface, the PEEM intensity was simultaneously averaged over the entire observation window by means of an electronic integrating device. The level of intensity was scaled such that a CO (oxygen) saturated surface corresponded to a value of 1 (0). From the resulting global signal $I(t)$, a reference value I_{ref} was then subtracted using a preset potentiometer. The reference value has been determined in the beginning of each series of experiments, before global delayed feedback was applied. It was chosen as the time average of the global PEEM intensity $I(t)$ in the initially developing state of spiral-wave turbulence. In the following step, the signal was delayed by a certain time τ_{d} using a computer. Afterwards, the delayed signal was electronically amplified by a factor determining the feedback intensity. A high-frequency filter was used to reduce electric noise and to invert the signal. Finally, the control signal was applied back to the system by controlling the automated inlet system for CO gas. The variation of the CO partial pressure p_{CO} in the reaction chamber followed the temporal modulations of the dosing rate with an additional delay $\tau_0 \approx 0.4$ s due to the finite response time of the inlet system and the residence time of gases in the pumped chamber.

Thus, a global delayed feedback could be artificially introduced, such that

$$p_{\mathrm{CO}}(t) = p_0 - \mu[I(t-\tau) - I_{\mathrm{ref}}], \tag{1}$$

where p_{CO} is the CO partial pressure in the reaction chamber, $I(t)$ denotes the integral PEEM intensity at time t, $\tau = \tau_0 + \tau_{\mathrm{d}}$ is the effective time delay, the parameter μ specifies the feedback intensity, and p_0 and I_{ref} are the CO partial pressure and the mean base level of the integral PEEM intensity in absence of feedback, respectively.

III. EXPERIMENTAL RESULTS

A. Overview

Multiple experiments have been conducted with different values of the feedback intensity μ and the delay τ. In the beginning of each series of experiments, the parameters of temperature and partial pressures have been chosen in such a way that the reaction was oscillatory and, furthermore, a complex state of chemical turbulence characterized by only short-scale spatial correlations developed in absence of feedback. A sequence of PEEM images showing the spontaneous development of chemical turbulence from a uniformly oxygen covered surface state is displayed in Fig. 1. A characteristic property of such turbulence is the spontaneous creation of irregular wave fronts and multiple fragments of rotating spiral waves. The spiral waves repeatedly undergo breakups, leading to the formation of new spiral fragments at different locations. This type of turbulence was found in a wide range of temperatures for an appropriate choice of the partial pressures of gases in the chamber.

Starting from the regime of spiral-wave turbulence, global delayed feedback according to Eq. (1) was switched on after some time, and its parameters could be varied. In experiments with a systematic variation of the feedback parameters μ and τ, we have observed that turbulence could be suppressed and replaced by stable uniform oscillations for any delay time (delays up to $\tau = 10$ s have been probed) provided that the feedback intensity μ was sufficiently high (up to 5×10^{-5} mbar, corresponding to CO partial pressure variations of about 20% in the state of synchronous oscillations). Usually, the synchronization threshold was significantly lower (about 5% variations in p_{CO}). The period of uniform oscillations was affected by the feedback and varied approximately between 3 s and 10 s, with a tendency to increase for

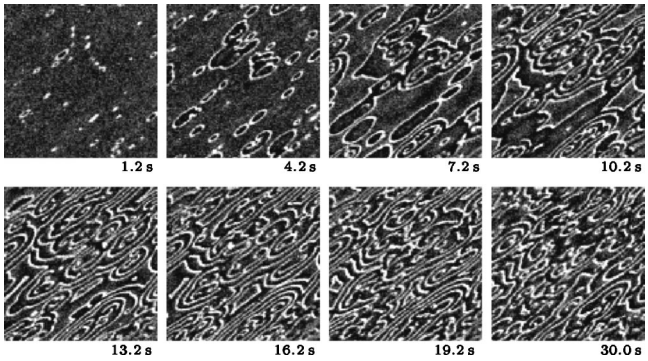

FIG. 1. Spontaneous development of spiral-wave turbulence from a uniformly oxygen covered surface state. The CO valve was initially kept closed and is opened at $t=0$ s. Eight subsequent snapshots of PEEM images of size 330×330 μm^2 are displayed. Dark areas in the images are predominantly oxygen covered while bright regions are mainly CO covered. The parameter values of temperature, oxygen partial pressure, and CO partial pressure are, respectively, $T=529$ K, $p_{O_2}=40.0\times10^{-5}$ mbar, and $p_{CO}=12.3\times10^{-5}$ mbar.

longer delays and decrease for stronger feedbacks.

For lower feedback intensities, the feedback does not transform spiral-wave turbulence into stable uniform oscillations but leads to the formation of novel spatiotemporal patterns. In the initial state of spiral-wave turbulence in absence of feedback, the integral PEEM intensity is almost constant except for small random fluctuations. As the feedback intensity is increased starting from zero, global oscillations set in, and turbulent spiral waves are first replaced by *intermittent turbulence*. This state is characterized by turbulent cascades of localized objects on a uniformly oscillating background. Intermittent turbulence is found for any choice of the time delay when the feedback intensity is increased from low values. Strong hysteresis is present at the transition from intermittent turbulence to uniform oscillations, that is, at a fixed time delay, uniform oscillation disappears at significantly lower values upon a decrease of the feedback intensity than they appear from intermittent turbulence upon an increase of μ.

By further increasing the feedback intensity from the state of intermittent turbulence, additional spatiotemporal patterns are observed below the transition to uniform oscillations for delays in the interval $0.5\ \mathrm{s}<\tau<1.0$ s. The precise stability regions of these patterns—*standing waves*, *cellular structures*, and *cluster patterns*—sensitively depend on the choice of temperature and partial pressures. In the following, we discuss the properties of the different types of structures observed. While only selected frames of patterns are presented here, short videos illustrating the evolution of different two-dimensional spatiotemporal patterns are available via Internet [27].

B. Intermittent turbulence

By fixing the feedback intensity below the transition to uniform oscillations, two different types of localized turbulent objects representing intermittent turbulence have been identified, namely, bubble-shaped structures and spiral-wave fragments. An example of the first type of intermittent turbulence is displayed in Fig. 2. The PEEM images in Fig. 2(a) are snapshots taken within one cycle of the pattern evolution. Starting from a dark, uniform state, bright spots develop at different locations. When the growing spots reach a certain size, darker regions develop in the middle of these objects, transforming them into ring-shaped structures. Because the wave back of the expanding rings propagates faster than the wave front, after some time the whole pattern fades away and is replaced by the uniform dark state. Then the entire cycle repeats.

The temporal evolution of the pattern is further analyzed in Fig. 2(c), showing the space-time diagram along the line AB indicated in the first image in Fig. 2(a). Expanding bubbles are represented by triangular structures in the cross section. Examining this diagram, it is found that the bubbles can die and reproduce. When the bubbles have reproduced until many of them are found, massive annihilation occurs and only a few of them survive. Thus, an irregular behavior of repeated reproduction cascades is observed. In a sequence of PEEM images taken at subsequent evolution cycles of the pattern, this behavior is reflected by a repeated alternation between system states with large and small fractions of the surface occupied by turbulent objects, see Fig. 2(b). In the example shown, the number and size of the turbulent bubbles typically vary on the time scale of about six evolution cycles. During intermittent turbulence, the variations of the CO partial pressure are aperiodic but rigidly correlated with the evolution cycles of the pattern, see the curves below the space-time diagram in Fig. 2(c) showing the temporal variations of CO pressure (black line) and negative integral PEEM intensity (gray line).

In addition to the turbulent bubble structures, a similar state of intermittent turbulence characterized by localized fragments of spiral waves has also been observed. This state predominantly occurred at higher values of temperature, where chemical turbulence in absence of feedback was more strongly developed and displayed a higher density of small spiral fragments. The localized spirals during intermittent turbulence undergo similar evolution cycles as the bubble structures. They also reproduce until they occupy almost the entire monitored surface area, and then annihilate such that only few of them survive. Typical PEEM images of spiral-wave fragments on the background of uniform oscillations are displayed in Fig. 3.

C. Standing waves

Like all structures described in the following, oscillatory standing waves were only found at delays in the interval $0.5\ \mathrm{s}<\tau<1.0$ s and at intermediate values of the feedback intensity. Four snapshots of a typical example of oscillatory standing waves are displayed in the top row of Fig. 4. Oscillatory standing waves are characterized by the repeated development of bright stripes from the dark uniform state. They form a spatially periodic array and, depending on the chosen parameters, have a wavelength of roughly 20–50 μm. Due to anisotropy of diffusion on the Pt(110) single-crystal surface, the stripes are mainly oriented into the direction of fast

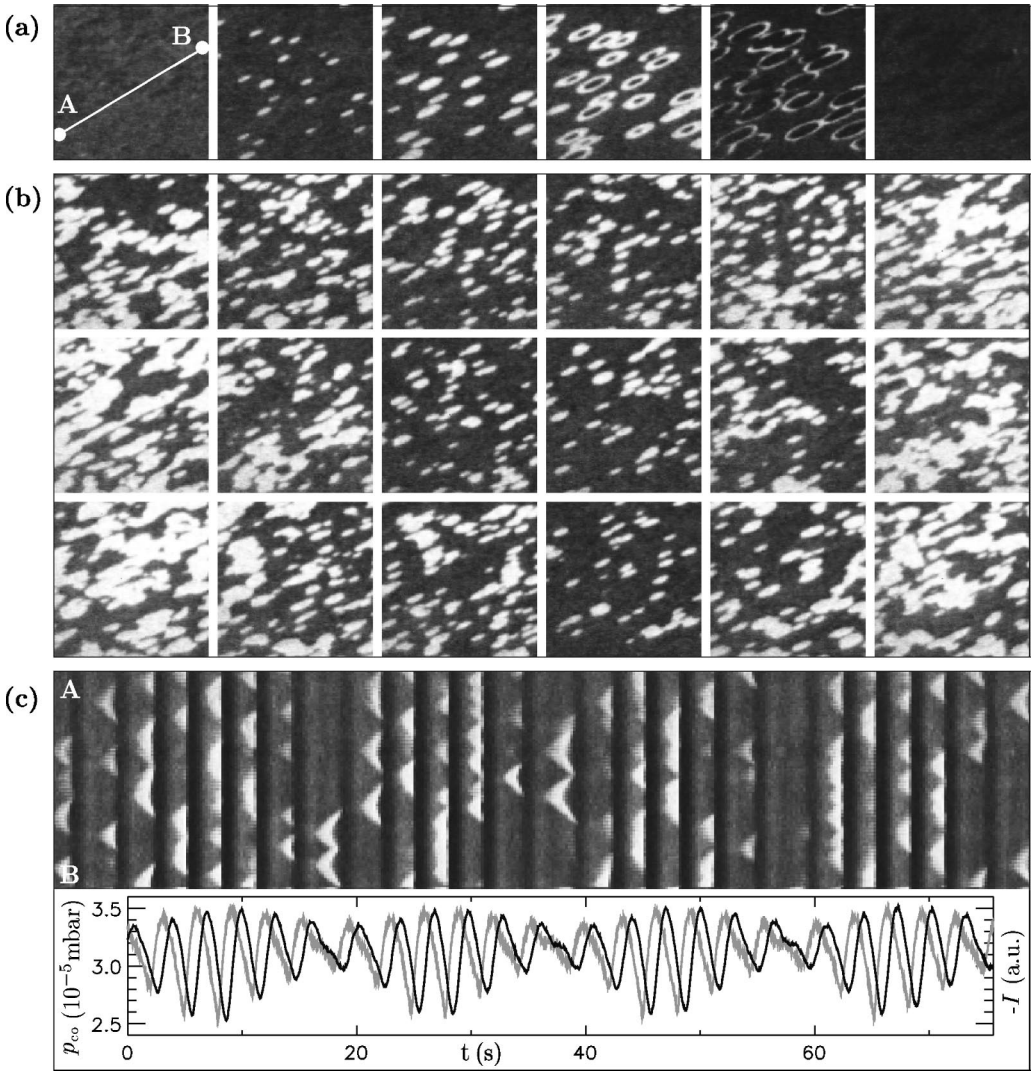

FIG. 2. Intermittent turbulence represented by reproducing and annihilating turbulent bubbles on the background of uniform oscillations. (a) Six subsequent PEEM images of size 360×360 μm^2 during a single cycle of local oscillations. The time interval between individual images is $\Delta t=0.7$ s. (b) Eighteen PEEM images shown at subsequent evolution cycles of the pattern (from left to right and top to bottom). The time interval between individual frames is $\Delta t\approx3.5$ s. (c) Evolution of the pattern along the line AB indicated in the first image in (a), and the corresponding temporal variations of CO partial pressure (black line) and negative integral PEEM intensity (gray line). The parameters are $T=495$ K, $p_{O_2}=10.0\times10^{-5}$ mbar, $p_0=3.15\times10^{-5}$ mbar, $\mu=2.0\times10^{-5}$ mbar, and $\tau=0.8$ s.

CO diffusion (the $[1\bar{1}0]$ direction). The stripes are only visible during relatively short intervals of each oscillation cycle. The space-time diagram in the middle row of Fig. 4 shows that the locations of stripes at subsequent oscillation cycles are shifted, so that a new stripe develops in the middle between two stripes seen in the previous cycle. Thus, the initial pattern is repeated after two periods of local oscillations. The periodic emergence of the spatial structure is rigidly correlated with the variations of CO partial pressure in the chamber, see the curves at the bottom of Fig. 4.

Standing waves with similar properties have been previously observed in CO oxidation on Pt(110) due to effects of intrinsic global gas phase coupling [21,25]. Under such conditions, they were seen only at relatively high temperatures (540–550 K), while in the present experiments, such structures have been observed also at significantly lower temperature values (down to $T=505$ K in the example shown in Fig. 4). Another difference is that under intrinsic global coupling, usually only a part of the catalytic surface was covered by the pattern of standing waves, while the rest of the area was in the state of uniform oscillations [25]. The pattern was always perfectly synchronized with the uniform oscillations and immediately broke down when the oscillations disappeared. Therefore, it was concluded that via the gas phase, uniform oscillations on other parts of the surface provided external forcing that acted on the standing waves and stabilized this pattern. In the presently reported experiments, the pattern was stabilized by the artificial global feedback, so that uniformly oscillating regions were not necessary for the occurrence of standing waves, and they usually occupied the entire monitored surface area. The required driving force could be simply generated by choosing a sufficiently large feedback intensity.

The repeated alternation of the stripe positions at subsequent oscillation cycles has been explained in the previous

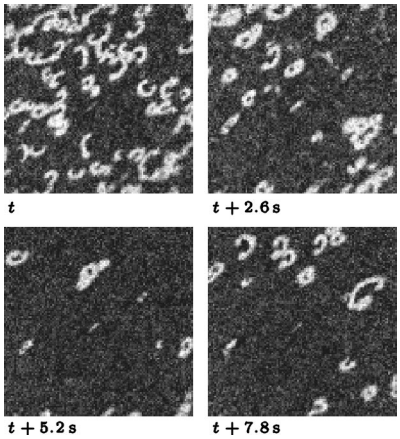

FIG. 3. Snapshots of intermittent turbulence represented by localized spiral fragments on a uniformly oscillating background. The images are 330×330 μm^2 in size. The parameters are $T=537$ K, $p_{O_2}=40.0\times10^{-5}$ mbar, $p_0=11.4\times10^{-5}$ mbar, $\mu=3.0\times10^{-5}$ mbar, and $\tau=0.7$ s.

studies [21,25] by periodic reflective collisions of traveling waves. The occurrence of such collisions has been attributed to the presence of subsurface oxygen. Alternating standing waves could be numerically reproduced in a model of CO oxidation on Pt(110) only by additionally taking into account the formation of subsurface oxygen [25]. Therefore, it seems likely that, at least to a small extent, subsurface oxygen was also present when standing waves were observed in the present experiments under artificial global feedback.

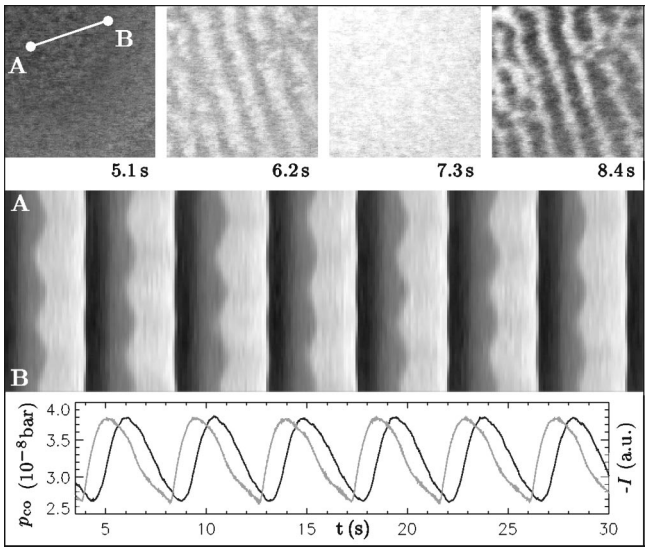

FIG. 4. Standing waves with an intrinsic wavelength. Displayed are four subsequent PEEM images of size 270×270 μm^2 during a single oscillation period (top), the evolution along the line AB indicated in the first image (middle), and the corresponding temporal variations of CO partial pressure (black line in the bottom) and negative integral PEEM intensity (gray line). The parameters are $T=505$ K, $p_{O_2}=10.0\times10^{-5}$ mbar, $p_0=3.30\times10^{-5}$ mbar, $\mu=1.6\times10^{-5}$ mbar, and $\tau=0.8$ s.

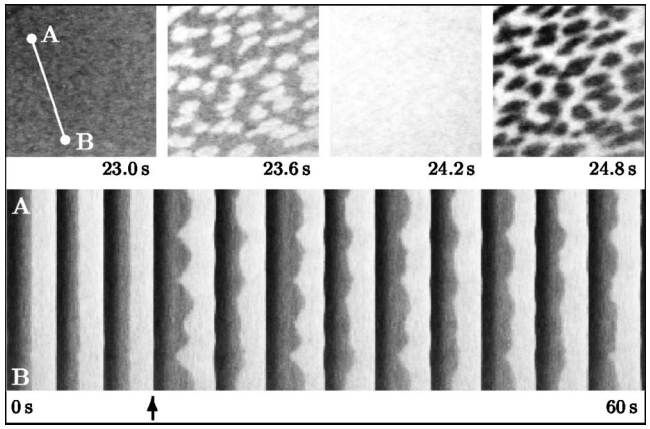

FIG. 5. Cellular structures and their development from standing waves. Displayed are four subsequent PEEM images of size 270×270 μm^2 during a single oscillation period (top), and the evolution along the line AB indicated in the first image (bottom). At the time moment indicated by an arrow, the feedback intensity has been instantaneously reduced from $\mu=1.6\times10^{-5}$ mbar to $\mu=1.1\times10^{-5}$ mbar. The other parameters are as in Fig. 4.

D. Cellular structures

A further type of pattern seen near the transition from turbulence to uniform oscillations is represented by oscillatory arrays of cells. Four snapshots of such a pattern, sampled within a single oscillation period, are displayed in the top row of Fig. 5. The cellular structure is visible only during short time intervals within each period. The appearance of cells at the transition from a predominantly oxygen covered to a mainly CO covered surface state is displayed in the second frame, and its recurrence during the transition back to an oxygen covered state is shown in the fourth frame in the top row of Fig. 5.

The space-time diagram in the lower part of Fig. 5 shows the development of the cellular structure from standing waves upon a sudden decrease of the feedback intensity at time $t=14$ s. The standing waves that were initially present are not seen in the space-time diagram because the cross section is chosen parallel to the orientation of the stripes.

Like standing waves, cellular structures usually occupy the entire imaged surface area. The local oscillations in this pattern are in harmonic resonance with the almost periodic variations of the global control signal. As a typical observation, the arrays of cells are fairly irregular. The irregularity may be explained as a representation of phase turbulence [28], a state characterized by small aperiodic variations of the oscillation phase in absence of amplitude defects. However, such irregularity may also, at least partly, be caused by the presence of small structural surface defects. No unambiguously regular, hexagonal cell arrays have been observed in the experiments described here.

Oscillatory cellular structures were also seen in previous measurements that employed mirror electron microscopy [29]. There, their presence was attributed to the action of intrinsic global gas phase coupling. The cell arrays were observed at relatively low values of temperature ($T\approx430$ K) and exhibited a temporal period of the order of 30 s and a

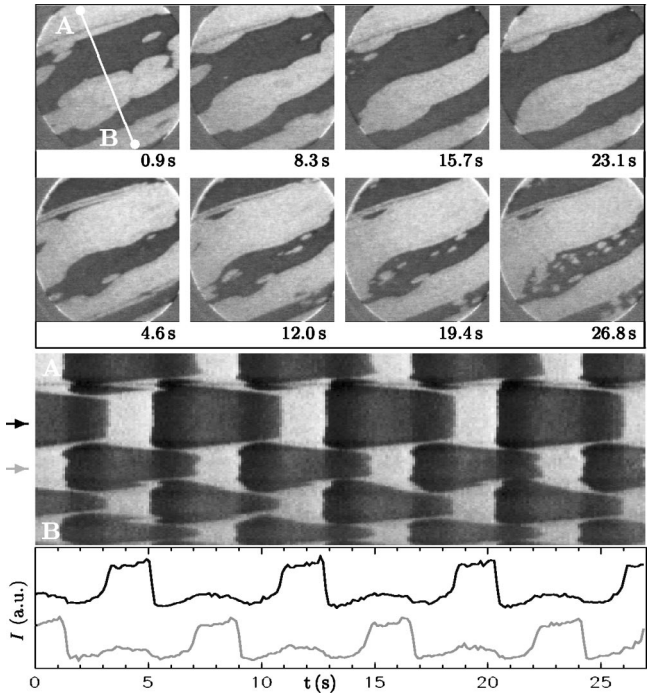

FIG. 6. Two-phase clusters. Displayed are subsequent PEEM images with a field of view of 500 μm in diameter (top), the evolution along the line *AB* indicated in the first image (middle), and the temporal variation of local PEEM intensity at the two different points indicated by arrows in the space-time diagram (bottom). The parameters are $T=500$ K, $p_{O_2}=10.0\times10^{-5}$ mbar, $p_0=3.07\times10^{-5}$ mbar, $\mu=0.6\times10^{-5}$ mbar, and $\tau=0.8$ s.

characteristic cell size of about 1 μm. In contrast, the artificially induced cellular structures described here were found at significantly higher temperature values (525–550 K) and typically exhibited an average cell size of ≈ 20 μm and an oscillation period of about 4 s.

E. Cluster patterns

When phase clusters develop, the catalytic surface splits into large regions belonging to either one of two different oscillatory states where frequencies are equal but phases are shifted by half a period. Usually, each of the two antiphase states occupies multiple spatial domains on the surface. An intrinsic spatial wavelength is missing in such a pattern. In the top and the second row of Fig. 6, snapshots of such a pattern are shown at time intervals of one oscillation period between subsequent frames within each row. Snapshots lying one upon the other are separated by half an oscillation period. Compared to the images shown in the top row, predominantly CO covered and oxygen covered regions have approximately interchanged in the second row. After a full period, the spatial distribution of the different domains is almost repeated.

The temporal evolution of the pattern along a cross section is shown in the space-time diagram in the middle of Fig. 6. It is seen that the shape of cluster domains undergoes small periodic variations. This breathing mode is rigidly correlated with the period of local oscillations in the pattern. On long time scales, the average locations of the interfaces between the antiphase domains are almost stationary or undergo only a weak drift.

Finally, the curves at the bottom of Fig. 6 display the temporal variations of the PEEM intensity at two sample points located within the opposite phase domains. The positions of the sample points are indicated by arrows on the left of the space-time diagram. Note that each maximum of PEEM intensity in the two curves is followed by a second, smaller peak, which indicates period-two oscillations. The local oscillation period is about twice the period of uniform oscillations occurring at a slightly increased feedback intensity. By analyzing the time series of local oscillations at sample points located within the small domain interfaces, it is found that the difference between subsequent oscillation maxima is strongly decreased there. The difference nearly vanishes in the center of an interface so that oscillations are almost simple periodic and have an intermediate amplitude.

Note that in the shown example of phase clusters, the total areas occupied by the antiphase domains within the observation window are almost equal or, in other words, the clusters show a state of phase balance. Phase balance for feedback-induced clusters has been predicted by theoretical modeling [15] and was also observed in CO oxidation experiments performed in a parameter regime where chemical turbulence was absent [16].

In a further set of experiments, we have explored the effects of a varied size of the feedback window on the developing patterns. In such experiments, not the integral PEEM intensity within the full observation window but the intensity integrated over a significantly smaller, rectangular region of the approximate size 250×180 μm^2 has been used for generation of the control signal. When the feedback parameters were then varied, we could not observe any significant qualitative differences between the types of patterns that formed inside and outside the feedback window. However, a subtle difference was observed for phase clusters, see Fig. 7. In Fig. 7(a), the feedback window that was used for generation of the control signal is indicated by a rectangular box. Interestingly, while phase clusters showed the property of phase balance within the feedback window, the total size of the different phase domains was generally not balanced outside this region. This difference becomes evident from the global oscillations of image intensity within and outside the feedback window, see Fig. 7(b). Inside the feedback window, the evenly weighted contributions of the local antiphase oscillations sum up to a periodic global signal of twice the frequency of local oscillations. In contrast, the contributions of the antiphase domains to the global oscillations are not balanced outside the rectangular region and thus, oscillations of the integral intensity have a twice larger period there. The lack of phase balance outside the feedback window can be understood from the following considerations: while a closed feedback loop acts on the patterns inside the feedback window and maintains the phase balance, the patterns outside this region are subject to external forcing through the independently generated control signal. Therefore, shape and size of the phase domains outside the feedback window are solely

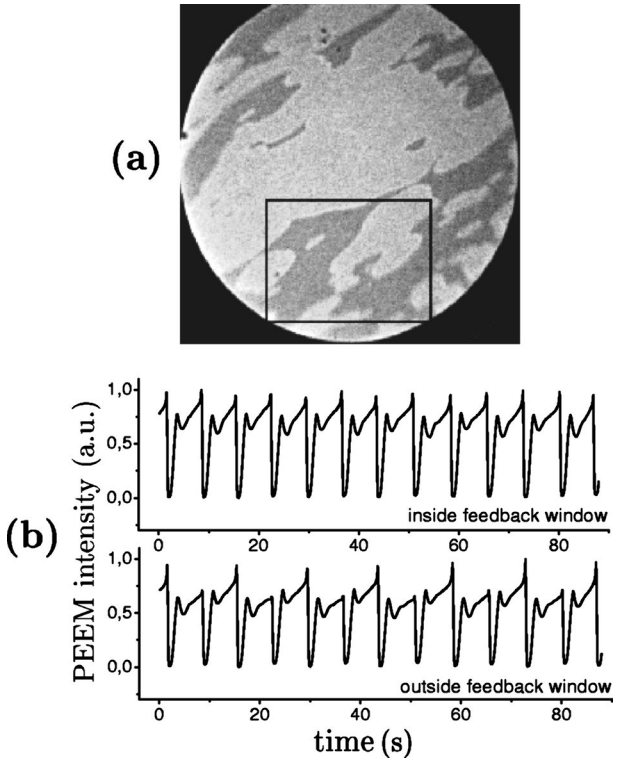

FIG. 7. (a) Snapshot of phase clusters in an experiment with a reduced feedback window indicated by the rectangular box. (b) Temporal variations of the negative integral PEEM intensity inside (upper curve) and outside (lower curve) the feedback window. The parameters are $T=524$ K, $p_{O_2}=10.0\times10^{-5}$ mbar, $p_0=3.10\times10^{-5}$ mbar, $\mu=3.3\times10^{-5}$ mbar, and $\tau=0.75$ s.

determined by the local initial conditions prior to the application of feedback.

IV. PATTERN CHARACTERIZATION

To further analyze the observed types of patterns, we have employed a variant of the *analytic signal approach* [30,31]. This method has allowed us to transform sequences of (typically 250) experimental PEEM images into time-dependent spatial distributions of phase and amplitude variables. For the local PEEM intensity $I(\mathbf{x},t)$ at an observation point $\mathbf{x}$, its Hilbert transform

$$\tilde{I}(\mathbf{x},t)=\pi^{-1}\int_{-\infty}^{\infty}(t-t')^{-1}I(\mathbf{x},t')dt' \tag{2}$$

was computed (this could be easily realized by determining the Fourier transform of I, shifting each complex Fourier coefficient by a phase of $\pi/2$, and performing the reverse Fourier transform [31,32]). This was repeatedly done for all pixels $\mathbf{x}$ in an 100×100 array covering the respective pattern. Using $I(\mathbf{x},t)$ and its Hilbert transform $\tilde{I}(\mathbf{x},t)$, a complex variable

$$\zeta(\mathbf{x},t)=I(\mathbf{x},t)+i\tilde{I}(\mathbf{x},t) \tag{3}$$

known as analytic signal [30] was defined.

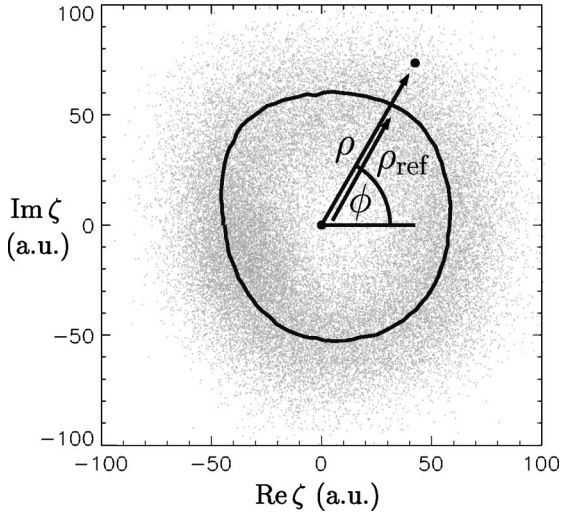

FIG. 8. Illustration of the transformation to the amplitude $R=\rho/\rho_{\mathrm{ref}}(\phi)$ and phase $\phi=\arg\zeta$ of local oscillations; the reference orbit $\rho=\rho_{\mathrm{ref}}(\phi)$ is indicated by the closed line.

Afterwards, the time-dependent spatial distributions of phase $\phi(\mathbf{x},t)$ and amplitude $R(\mathbf{x},t)$ were determined from the analytic signal in the following way. The phase was directly computed as $\phi=\arg\zeta$, thus representing the polar angle in the plane spanned by the variables I and $\tilde{I}$. The amplitude was defined as $R=\rho/\rho_{\mathrm{ref}}(\phi)$, where $\rho=|\zeta|$ is the standard definition of the amplitude modulus within the analytic signal approach. The normalization to $\rho_{\mathrm{ref}}(\phi)$ was introduced to approximately compensate for deviations from harmonicity in the observed oscillations. To obtain $\rho_{\mathrm{ref}}(\phi)$, the statistical distribution of $\zeta(\mathbf{x},t)$ for all 100×100 pixels and at all 250 time moments was plotted into the complex plane, as illustrated in Fig. 8 for a set of spatiotemporal data representing a pattern of spiral-wave turbulence. The reference amplitude $\rho_{\mathrm{ref}}(\phi)$ was then determined as the statistical average of $\rho=|\zeta|$ inside each of 200 equidistant narrow intervals of the polar angle ϕ. Note that the closed curve $\rho=\rho_{\mathrm{ref}}(\phi)$ in the complex plane can be viewed as representing a reference orbit of the system deduced from the experimental data. In this way, a different characteristic reference orbit has been generated for each set of spatiotemporal data to which the variable transformation was applied.

By applying this transformation separately to each of the different types of experimentally observed patterns presented in Sec. III, time-dependent spatial distributions of phase ϕ and amplitude R in each pattern have been constructed. In Fig. 9, we show snapshots of PEEM images (top row) for various observed patterns, and corresponding snapshots of the phase (second row) and amplitude distributions (third row). Additionally, the bottom row of Fig. 9 shows a phase portrait of each pattern, obtained by displaying the amplitudes and phases for all resolving pixels in polar coordinates. The phase ϕ of a point is represented by the polar angle and the amplitude R is the distance to the coordinate origin.

In spiral-wave turbulence [Fig. 9(a)], the fluctuations of amplitude and phase are strong, as indicated by the broadband structure in the phase portrait. For intermittent turbu-

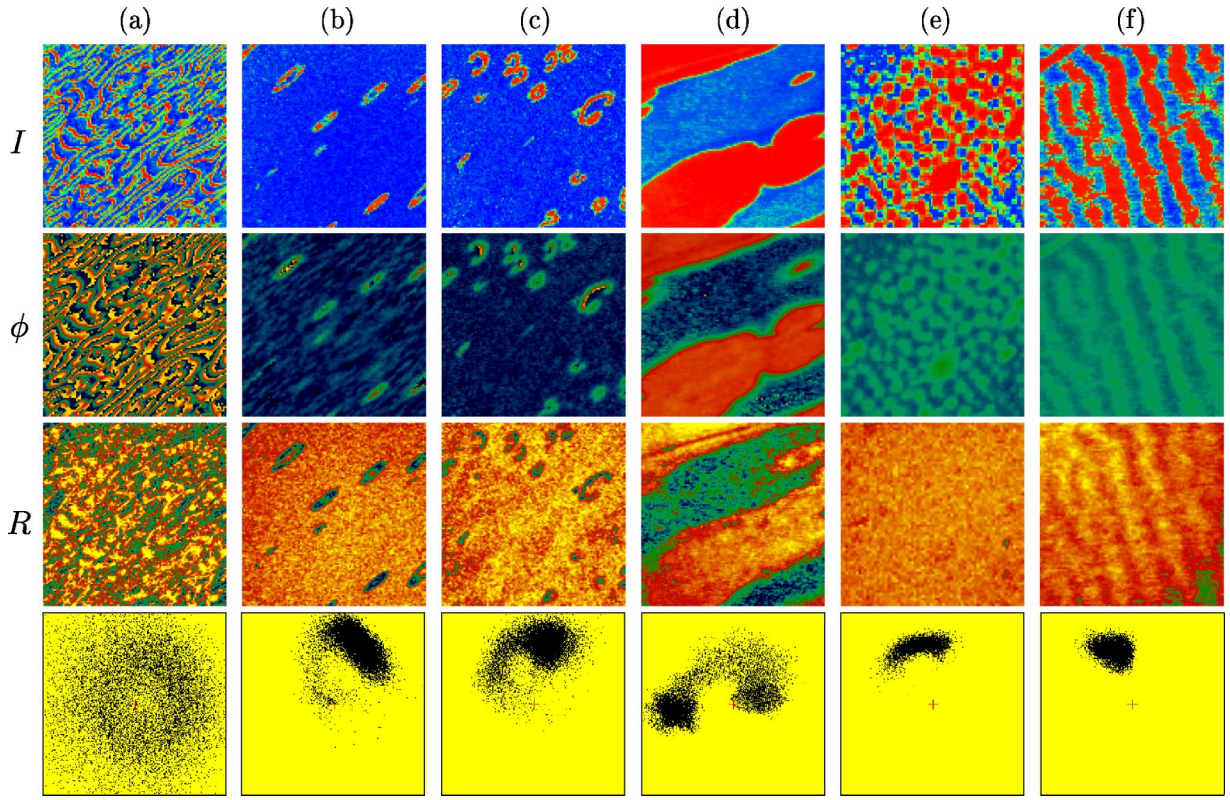

FIG. 9. (Color online) (a)–(f) PEEM images (top row), distributions of phase (second row), amplitude (third row), and phase portraits (bottom row) for several typical patterns observed in CO oxidation experiments. In the PEEM images, blue (dark gray) color denotes surface areas predominantly covered by oxygen, and red (light gray) regions are mainly CO covered. Green (bright) color denotes intermediate values of intensity. In the phase and amplitude representations, yellow (bright) color denotes high, and blue (dark) color denotes low values. Green and red (gray) areas denote intermediate phase and amplitude values. The parameter values of temperature (K), oxygen partial pressure (10^{-5} mbar), base CO pressure p_0 (10^{-5} mbar), feedback intensity μ (10^{-5} mbar), and delay time τ (s) are, respectively, (a) 529, 40.0, 12.3, 0, 0; (b) 540, 40.0, 13.1, 1.7, 0.7; (c) 537, 40.0, 11.4, 3.0, 0.7; (d) 500, 10.0, 3.1, 0.6, 0.8; (e) 535, 40.0, 12.2, 4.0, 0.6; and (f) 505, 10.0, 3.3, 1.6, 0.8. The side length of images is (a),(c),(d) 330 μm, (b) 360 μm, (e) 210 μm, and (f) 270 μm.

lence [Figs. 9(b) and 9(c)], amplitude and phase are almost constant in the main part of the medium where uniform oscillations take place. The amplitude is significantly decreased in the bubble-shaped objects [Fig. 9(b)] and small localized spirals [Fig. 9(c)], so that they represent extended amplitude defects. Perpendicular to such objects, the oscillation phase varies rapidly in space. The phase portraits of intermittent turbulence show a spot corresponding to the uniform state of the medium and a tail corresponding to the amplitude defects. When cluster patterns [Fig. 9(d)] develop, the medium breaks into two phase states seen as spots in the corresponding phase portrait. The amplitudes of the two oscillatory states differ because the local oscillations exhibit period-two behavior. The ''bridge'' in the phase portrait connecting the two spots corresponds to the interfaces between the cluster domains; note that the phase varies smoothly and the amplitude is not significantly reduced at the interface for such cluster patterns. In cellular structures [Fig. 9(e)], small phase modulations are observed, while the amplitude remains approximately constant. In standing waves [Fig. 9(f)], both the phase and the amplitude are periodically modulated.

V. CONCLUSIONS

In this paper, feedback-induced pattern formation in CO oxidation on Pt(110) has been experimentally studied in a parameter regime where the unperturbed reaction exhibited chemical turbulence. By applying strong global delayed feedbacks, turbulence could be completely suppressed, leading to uniform oscillations. A large variety of complex spatiotemporal patterns was found when global delayed feedback was used to bring the system to the boundary between regular and chaotic dynamics. A particularly interesting result is the experimental observation of intermittent turbulence. This state is characterized by cascades of reproducing and annihilating turbulent bubble structures or small localized spirals on a background of uniform oscillations. Standing waves and oscillating cellular structures represent further interesting structures resulting from the action of global delayed feedback. Finally, phase clusters with period-two local oscillation dynamics could be induced. In additional experiments with a reduced feedback window, we have shown that phase balance is a characteristic property of phase clusters developing under global feedback but does not occur under periodic, state-independent forcing. Our experimental observations agree well with the results of a theoretical study [33] that explores pattern formation in a realistic model of CO oxidation on Pt(110) under global delayed feedback.

To further characterize the observed patterns, we have processed the experimental data to approximately reconstruct

amplitude and phase variables. This representation allows to directly compare the properties of patterns in systems of different origins and provides a link to previous general studies [9,10] of global feedbacks in oscillatory turbulent systems performed in the framework of the complex Ginzburg-Landau equation (CGLE). The CGLE is the amplitude equation of a field of diffusively coupled Hopf oscillators and describes small-amplitude harmonic oscillations. The oscillations in our experiments were nonharmonic and the system was not close to a supercritical Hopf bifurcation. Nonetheless, the results of our investigations show remarkable agreement with the theoretical predictions of Refs. [9,10] where intermittent turbulence characterized by cascades of ring-shaped amplitude defects, oscillatory cellular arrays, and clusters were also found. This indicates that the observed effects of pattern formation near the edge of chaos may be typical for a broad class of reaction-diffusion systems.

We finally note that cluster patterns similar to those reported here have also been experimentally observed in the light-sensitive Belousov-Zhabotinsky (BZ) reaction under global feedback [13,17] and periodic external forcing [34,35]. In these studies, however, chemical turbulence was absent in the unperturbed system and consequently, neither the states of intermittent turbulence nor irregular cellular structures (which can be interpreted as a representation of phase turbulence) have been reported. Since turbulent states do exist in the BZ reaction [36–39], it would be interesting to see whether such types of patterns can also be induced near the edge of chaos in this and in other reactions.

ACKNOWLEDGMENTS

We acknowledge financial support of the Deutsche Forschungsgemeinschaft in the framework of the Sonderforschungsbereich 555 ''Complex Nonlinear Processes.'' We thank I. G. Kevrekidis for assistance with the microlithographic fabrication of the crystal samples.

[1] E. Ott, C. Grebogi, and J.A. Yorke, Phys. Rev. Lett. **64**, 1196 (1990).
[2] K. Pyragas, Phys. Lett. A **170**, 421 (1992).
[3] M. Münkel, F. Kaiser, and O. Hess, Phys. Rev. E **56**, 3868 (1997).
[4] T. Pierre, G. Bonhomme, and A. Atipo, Phys. Rev. Lett. **76**, 2290 (1996).
[5] G. Franceschini, S. Bose, and E. Schöll, Phys. Rev. E **60**, 5426 (1999).
[6] O. Beck, A. Amann, E. Schöll, J.E.S. Socolar, and W. Just, Phys. Rev. E **66**, 016213 (2002).
[7] W. Wang, I.Z. Kiss, and J.L. Hudson, Phys. Rev. Lett. **86**, 4954 (2001).
[8] M. Kim, M. Bertram, M. Pollmann, A. von Oertzen, A.S. Mikhailov, H.H. Rotermund, and G. Ertl, Science **292**, 1357 (2001).
[9] D. Battogtokh and A.S. Mikhailov, Physica D **90**, 84 (1996).
[10] D. Battogtokh, A. Preusser, and A.S. Mikhailov, Physica D **106**, 327 (1997).
[11] K. Krischer and A. Mikhailov, Phys. Rev. Lett. **73**, 3165 (1994).
[12] O.-U. Kheowan, C.-K. Chan, V.S. Zykov, O. Rangsiman, and S.C. Müller, Phys. Rev. E **64**, 035201(R) (2001).
[13] V.K. Vanag, L. Yang, M. Dolnik, A.M. Zhabotinsky, and I.R. Epstein, Nature (London) **406**, 389 (2000).
[14] L. Yang, M. Dolnik, A.M. Zhabotinsky, and I.R. Epstein, Phys. Rev. E **62**, 6414 (2000).
[15] M. Bertram and A.S. Mikhailov, Phys. Rev. E **63**, 066102 (2001).
[16] M. Pollmann, M. Bertram, and H.H. Rotermund, Chem. Phys. Lett. **346**, 123 (2001).
[17] V.K. Vanag, A.M. Zhabotinsky, and I.R. Epstein, J. Phys. Chem. A **104**, 11566 (2000).
[18] R. Imbihl and G. Ertl, Chem. Rev. **95**, 697 (1995).
[19] T. Engel and G. Ertl, Adv. Catal. **28**, 1 (1979).
[20] T. Gritsch, D. Coulman, R.J. Behm, and G. Ertl, Phys. Rev. Lett. **63**, 1086 (1989).
[21] S. Jakubith, H.H. Rotermund, W. Engel, A. von Oertzen, and G. Ertl, Phys. Rev. Lett. **65**, 3013 (1990).
[22] M. Falcke, H. Engel, and M. Neufeld, Phys. Rev. E **52**, 763 (1995).
[23] M. Falcke and H. Engel, Phys. Rev. E **56**, 635 (1997).
[24] M. Falcke and H. Engel, J. Chem. Phys. **101**, 6255 (1994).
[25] A. von Oertzen, H.H. Rotermund, A.S. Mikhailov, and G. Ertl, J. Phys. Chem. B **104**, 3155 (2000).
[26] H.H. Rotermund, Surf. Sci. Rep. **29**, 265 (1997).
[27] M. Bertram, C. Beta, M. Pollmann, A.S. Mikhailov, H.H. Rotermund, and G. Ertl, videos of spatiotemporal patterns in experiments with CO oxidation under global delayed feedback, in http://www.fhi-berlin.mpg.de/~complsys
[28] P. Manneville and H. Chaté, Physica D **96**, 30 (1996).
[29] K.C. Rose, D. Battogtokh, A. Mikhailov, R. Imbihl, W. Engel, and A.M. Bradshaw, Phys. Rev. Lett. **76**, 3582 (1996).
[30] P. Panter, *Modulation, Noise, and Spectral Analysis* (McGraw-Hill, New York, 1965).
[31] M. Rosenblum and J. Kurths, in *Nonlinear Analysis of Physiological Data*, edited by H. Kantz, J. Kurths, and G. Mayer-Kress (Springer, Berlin, 1998), p. 91.
[32] M.G. Rosenblum, A.S. Pikovsky, and J. Kurths, Phys. Rev. Lett. **76**, 1804 (1996).
[33] M. Bertram and A.S. Mikhailov, Phys. Rev. E. **67**, 036207 (2003).
[34] V. Petrov, Q. Ouyang, and H.L. Swinney, Nature (London) **388**, 655 (1997).
[35] A.L. Lin, M. Bertram, K. Martinez, H.L. Swinney, A. Ardelea, and G.F. Carey, Phys. Rev. Lett. **84**, 4240 (2000).
[36] Q. Ouyang and J.-M. Flesselles, Nature (London) **379**, 143 (1996).
[37] Q. Ouyang, H.L. Swinney, and G. Li, Phys. Rev. Lett. **84**, 1047 (2000).
[38] L.Q. Zhou and Q. Ouyang, Phys. Rev. Lett. **85**, 1650 (2000).
[39] L.Q. Zhou and Q. Ouyang, J. Phys. Chem. A **105**, 112 (2001).